Volume 17, Number 3, 2024. pp. 291-298

Jordan Journal of Physics

ARTICLE

Some Phenomenological Aspects of Higgs Production in Two Leptons and $b\bar{b}$ Final State Processes

Aissa Belhouari

Department of Physics, Faculty of Exact Science and Computing, Chemin des Cretes ex INEX 27000 University Abd el Hamid Ibn Badis-Mostaganem, Algeria.

Doi: **https://doi.org/10.47011/17.3.4**

Received on: 22/06/2022; *Accepted on: 30/10/2022*

Abstract: We present a partonic-level analysis of the two leptons and $b\bar{b}$ final states processes at the ILC $e^+e^- \to e^+e^-b\bar{b}$. This process contains Higgs production with an electron-positron pair, where the Higgs decays into a $b\bar{b}$ quark pair as a sub-process, $e^+e^- \to e^+e^-H \to e^+e^-b\bar{b}$. We tried to isolate this sub-process with a minimum set of cuts. Particularly, cross-sections are estimated at different energies, and the main distributions of kinematic variables characterizing the process are derived using the software Calchep [16]. The results provide information on signal and background characteristics for different ILC operating stages.

Keywords: Higgs physics at ILC, Higgsstrahlung process, ZZ fusion process, Calchep.

1. Introduction

The discovery of the Higgs particle at the LHC by the Atlas and CMS collaborations [1, 2] has constituted a starting point of an extensive Higgs physics program aimed at determining its principal properties. LHC data have allowed the determination of the spin, charge, and parity which are not enough to confirm it as the SM Higgs because other models predict scalars with the same properties [3]. The couplings and width are poorly constrained and require high precision measurements since BSM physics predicts a few percent deviation from their SM values.

One of the main fields of focus for the next generation of colliders is to perform high-precision Higgs physics experiments. With a precise initial state energy and a clean environment with respect to the LHC, because of the low QCD background, the ILC is without doubt the ideal machine to achieve this goal [4-6]. The three principal Higgs production channels are: Higgsstrahlung $e^+e^- \to ZH$, WW fusion $e^+e^- \to W^+W^-\nu\bar{\nu} \to H\nu\bar{\nu}$, and ZZ fusion $e^+e^- \to ZZe^+e^- \to e^+e^-H$, whose lowest order diagrams are illustrated in Fig.1.

To measure such Higgs properties as the Higgs mass and width or the HZZ coupling at ILC, several studies have focused mainly on the Higgsstrahlung process using the mass recoil variable to extract these properties in a model-independent way (an inclusive Higgs production) [7-14]. The recoil mass technique is based on measuring the decay products of the Z boson, which recoils against the Higgs boson independently of the Higgs decay mode. One gets a better signal selection efficiency, especially when only leptonic Z decays are considered [10].

$$e^+e^- \to (Z \to l^+l^-)(H \to X) \to l^+l^-X \qquad (1)$$

The recoil mass is given by the expression:

$$M^2_{rec} = S + \sqrt{S}\,E_{l^+l^-} + M^2_{l^+l^-} \qquad (2)$$

Corresponding Author: Aissa Belhouari **Email**: aissa.belhouari@univ-mosta.dz

where S is the center of mass energy squared, E_l+l- and M_l+l- are the energy and the invariant mass of the lepton pair, respectively. The M_{rec} distribution peaks at the Higgs mass (Fig. 2), from which the signal yield can be extracted. The $e^+e^- \rightarrow ZH$ cross section is maximal at 250 GeV, [8, 10, 13] but at higher energies, other channels become important, like Higgs production via ZZ fusion $e^+e^- \rightarrow ZZe^+e^- \rightarrow e^+e^-H$ [14, 15], as can be seen in Fig. 4 and Table 1.

Figure 4 shows a comparison between the Higgsstrahlung cross-section $\sigma(e^+e^- \rightarrow ZH \rightarrow e^+e^-H)$ and the total $\sigma(e^+e^- \rightarrow e^+e^-H)$ computed with unpolarized beams.

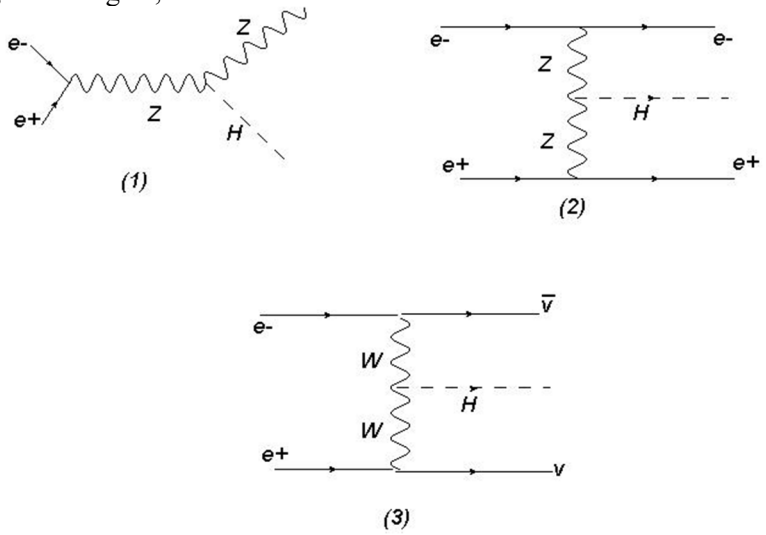

FIG. 1. Feynman diagrams for the three principal Higgs production channels at ILC: (1) Higgsstrahlung, (2) ZZ fusion, and (3) WW fusion.

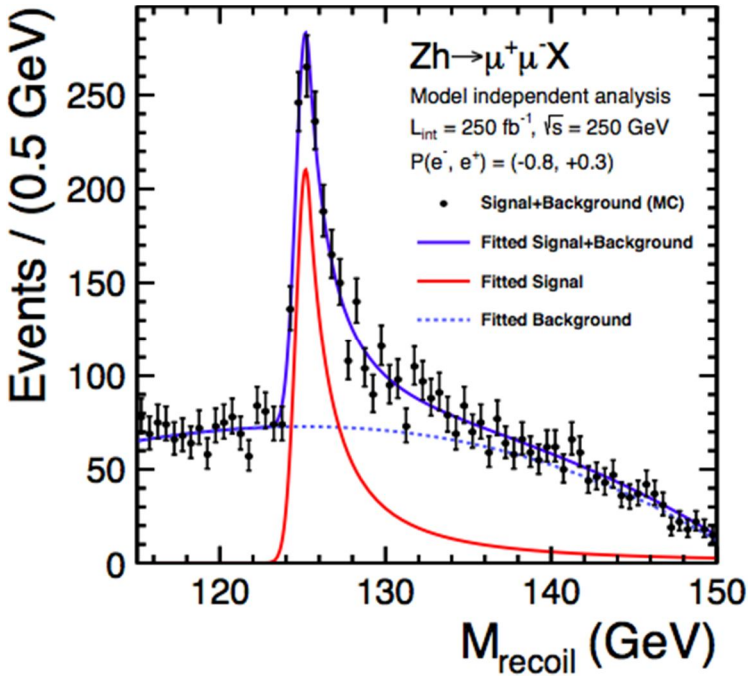

FIG. 2. Recoil mass distribution of $e^+e^- \rightarrow ZH$ followed by $Z \rightarrow \mu^+\mu^-$ at 250 GeV with a Higgs mass of 125 GeV taken from Ref. [5].

Their values and ratios at 250, 500, and 1000 GeV are also reported in Table 1. This confirms the results obtained in previous work [14]. For the Higgs mass of 125 GeV, the highest branching ratio is Br($H \rightarrow b\bar{b}$).

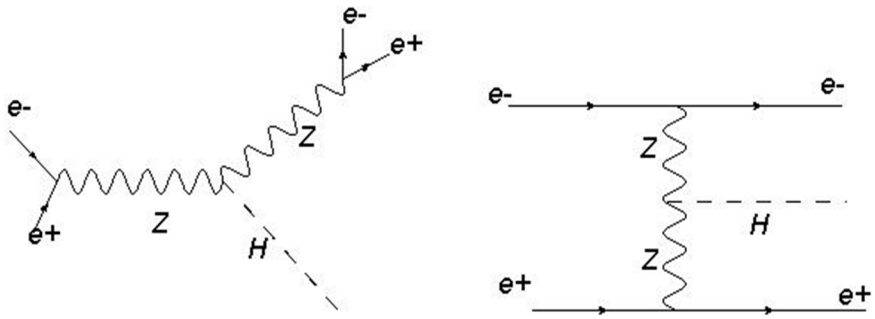

FIG. 3. Feynman diagrams of the process e+e− → e+e−H.

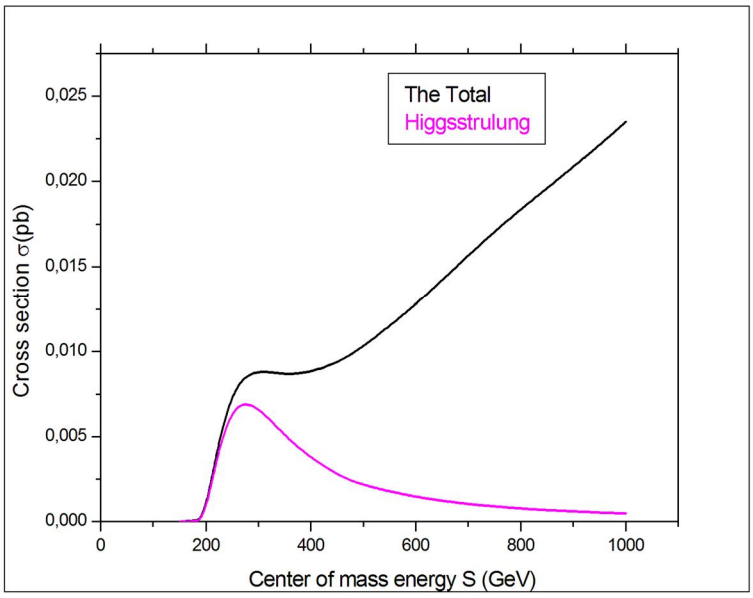

FIG. 4. Cross sections of the Higgsstrahlung and the total processes as a function of the CM energy.

TABLE 1. Cross sections of the Higgsstrahlung and the total processes as a function of the CM energy.

CM energy (GeV)	Total cross sec (pb)	Higgsstrahlung cross sec (pb)	Ratio
250	9.60×10^{-3}	8.75×10^{-3}	1.1
500	1.03×10^{-2}	2.13×10^{-3}	4.8
1000	2.35×10^{-2}	4.78×10^{-4}	49

Because of their high statistics and the b tagging and lepton identification capabilities of ILC, processes where the Higgs is produced with a pair of leptons, followed by a Higgs decay to a b quarks pair, $e^+e^- \rightarrow l^+l^-H \rightarrow l^+l^-b\bar{b}$, are particularly interesting.

2. Results and Analysis

In most analyses, the production times decay approximation ($\sigma \cdot Br$) is commonly used since it makes calculations simpler. However, this approach sacrifices valuable information and ignores the irreducible background, which may be significant. In this analysis, we used the Calchep software [16] (see appendix) to make a complete and exact computation of cross-sections and distributions for different kinematical variables of the process $e^+e^- \rightarrow e^+e^-b\bar{b}$, as illustrated in Figs. 5 and 6.

We are interested especially in the subprocess $e^+e^- \rightarrow e^+e^-H \rightarrow e^+e^-b\bar{b}$, which constitutes the signal, as depicted in Fig. 5. The irreducible background is represented by the diagrams in Fig. 6. One has to permute the e^+e^- and $b\bar{b}$ pairs in the diagrams (1) and (2) and attach the Z and photon propagator to the different legs in (3).

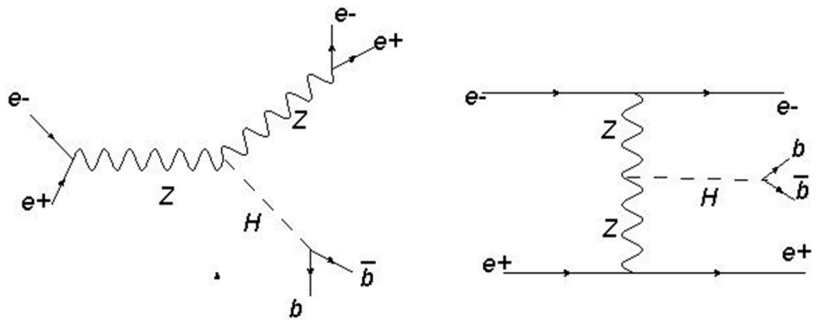

FIG. 5. Feynman diagrams of the signal.

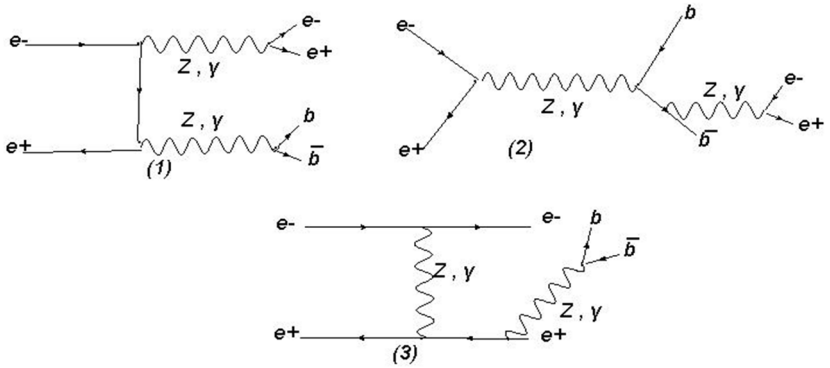

FIG. 6. Feynman diagrams of the background.

To extract the signal, we applied a cut on the $b\bar{b}$ invariant mass. It must be within the window $Mh - 10 < M(b\bar{b}) < Mh + 10$ where $Mh = 125$ GeV is the Higgs mass. Additionally, we applied cuts on the electron and positron transverse momentum $P_t > 10$ GeV and their invariant mass $M(e^+e^-) > 20$ GeV. These cuts serve to avoid the pole $q^2 = 0$ of the photon propagator because we are considering the electron and the positron as massless. We computed the cross-sections and obtained distributions of different kinematical variables, especially electron and b-quark rapidity and energy, both with the $M(b\bar{b})$ cut applied (signal) and without this cut (total = signal + background) at different energies (250 GeV, 500 GeV, and 1 TeV).

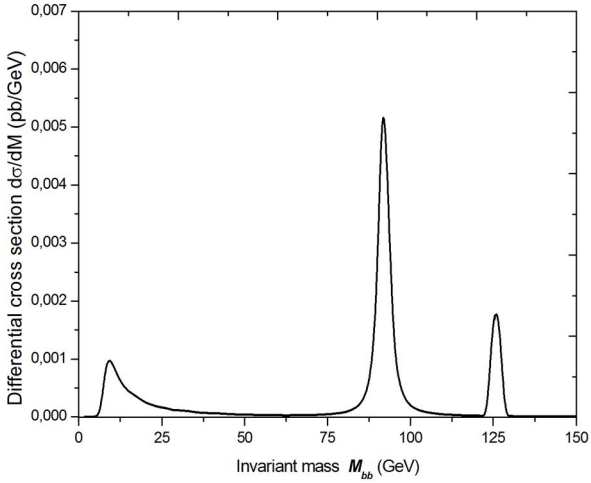

FIG. 7. The invariant mass distribution of the $b\bar{b}$ quarks pair shows the signal peak at 125 and the two background peaks: the Z peak and the low M peak.

TABLE 2. The computed cross sections with the M($b\bar{b}$) cut (signal) and without it (total).

CM Energy (GeV)	Signal (pb) (S)	Signal + Background (pb) (S+B)	Ratio S/(S+B)
250	6.36×10^{-3}	4.66×10^{-2}	0.136
500	7.15×10^{-3}	6.32×10^{-2}	0.113
1000	1.63×10^{-2}	9.05×10^{-2}	0.180

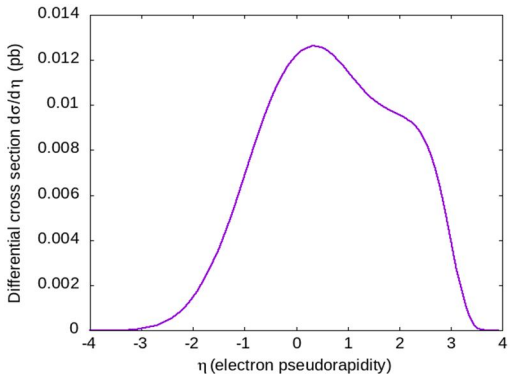

FIG. 8. Pseudorapidity distribution of the electron at 250 GeV without the $M(b\bar{b})$ cut.

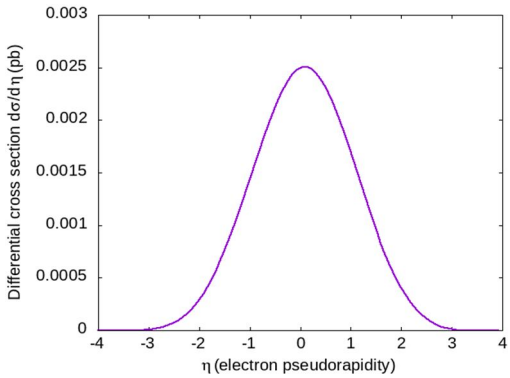

FIG. 9. Pseudorapidity distribution of the electron at 250 GeV with the $M(b\bar{b})$ cut.

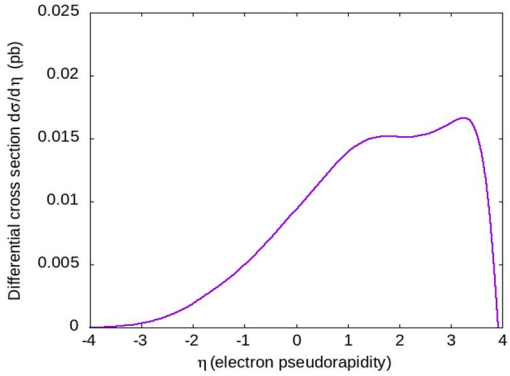

FIG. 10. Pseudorapidity distribution of the electron at 500 GeV without the $M(b\bar{b})$ cut.

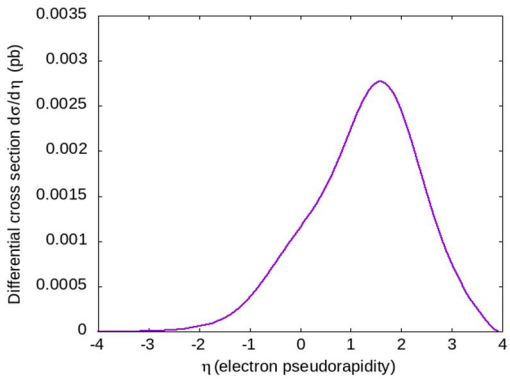

FIG. 11. Pseudorapidity distribution of the electron at 500 GeV with the $M(b\bar{b})$ cut.

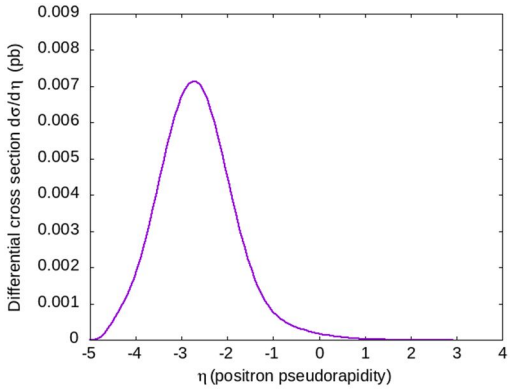

FIG. 12. Pseudorapidity distribution of the positron at 1 TeV with the $M(b\bar{b})$ cut.

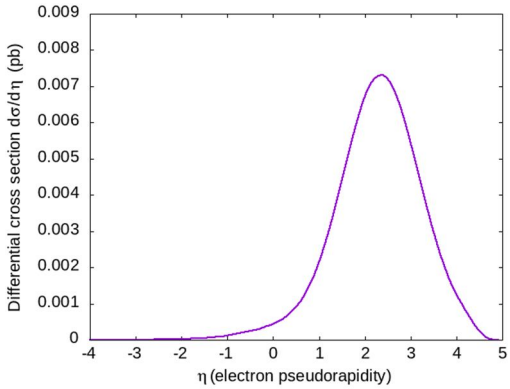

FIG. 13. Pseudorapidity distribution of the electron at 1 TeV with the $M(b\bar{b})$ cut.

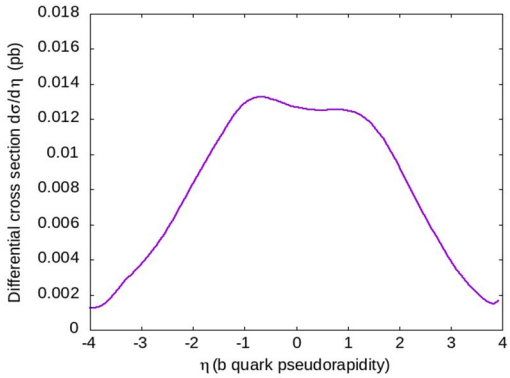

FIG. 14. Pseudorapidity distribution of the b jets at 500 GeV without the $M(b\bar{b})$ cut.

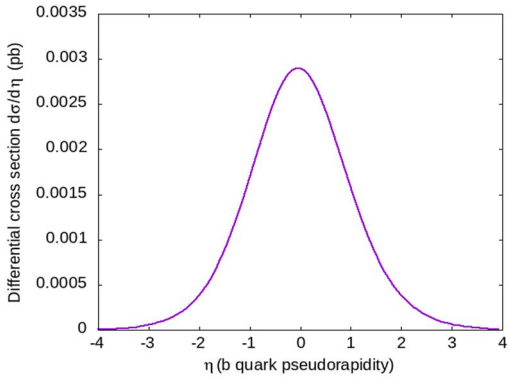

FIG. 15. Pseudorapidity distribution of the b jets at 500 GeV with the $M(b\bar{b})$ cut.

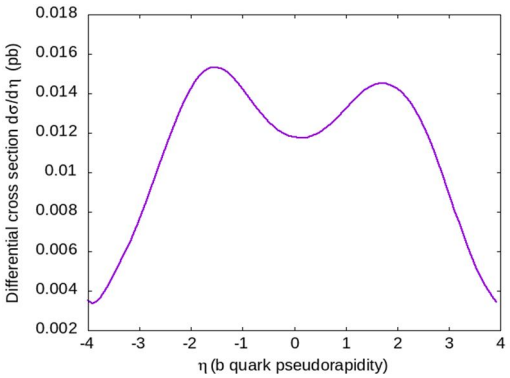

FIG. 16. Pseudorapidity distribution of the b jets at 1 TeV without the $M(b\bar{b})$ cut.

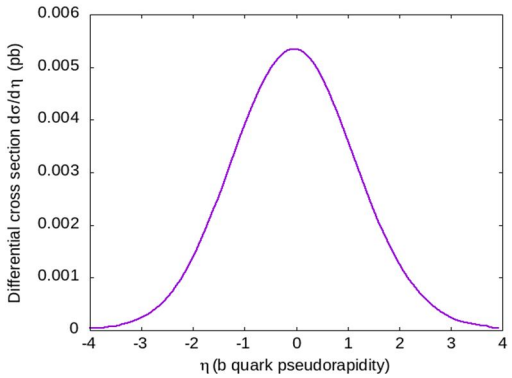

FIG. 17. Pseudorapidity distribution of the b jets at 1 TeV with the $M(b\bar{b})$ cut.

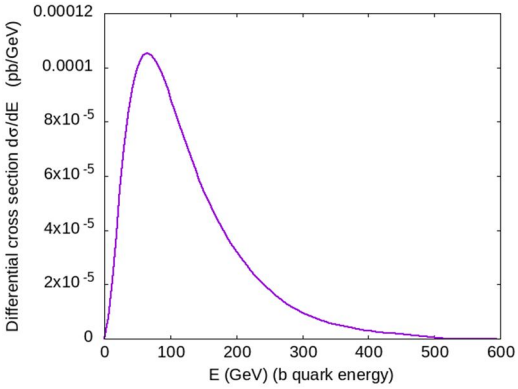

FIG. 18. Energy distribution of the b jets at 1 TeV with the $M(b\bar{b})$ cut.

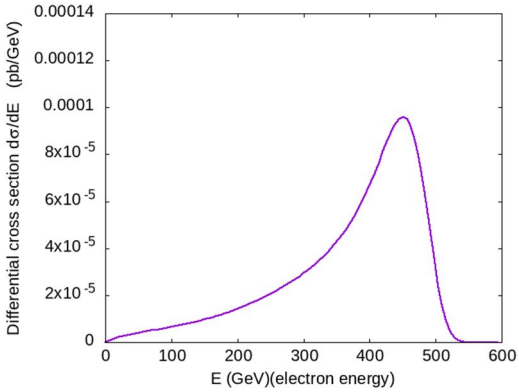

FIG. 19. Energy distribution of the electron at 1 TeV with the $M(b\bar{b})$ cut.

3. Conclusion

The signal $e^+e^- \to e^+e^-H \to e^+e^-b\bar{b}$ receives contributions from Higgsstrahlung $e^+e^- \to ZH \to e^+e^-b\bar{b}$ and ZZ fusion processes $e^+e^- \to e^+e^-ZZ \to e^+e^-H \to e^+e^-b\bar{b}$. Higgsstrahlung is an s-channel process, whereas Z vector boson fusion is a t-channel process. As the center of mass energy s increases, the Higgsstrahlung cross-section decreases as 1/s, but the Z-boson fusion production cross-section grows logarithmically.

The ILC operation starts with the collision energy of 250 GeV (just above the threshold for HZ production), where the Higgsstrahlung process is dominant and the contributions of the fusion processes are small. At higher energies, the Z-boson fusion cross-section becomes larger than the Higgsstrahlung cross-section for s > 450 GeV, and at s = 1 TeV the Z-boson fusion is dominant, as shown in Fig. 4 and Table 1. Figure 7 displays the $b\bar{b}$ invariant mass distributions, illustrating that the background is not negligible, This is evident from a comparison of the M_h peak (signal) with the Z and the low-value $M(b\bar{b})$ peaks (background). The largest background is $e^+e^- \to ZZ \to e^+e^-b\bar{b}$. As a consequence, the $M(b\bar{b})$ is efficient in eliminating the irreducible background by reducing events from non-Higgs processes. At the starting energy of 250 GeV, the Higgs is predominantly produced by the process $e^+e^- \to ZH \to e^+e^-b\bar{b}$. The signal is characterized by a central electron (positron) as shown in Fig. 9, and two central b jets from Higgs decays to $b\bar{b}$, with their invariant mass consistent with the Higgs because of the Higgsstrulung dominance. The background contains events with larger electron and positron pseudorapidity values $|\eta| > 2$ (forward electrons, backward positrons), as depicted in Fig. 8.

At higher energies, 500 GeV and 1 TeV, the ZZ fusion process becomes dominant. In this regime, the Higgs is primarily produced by the process $e^+e^- \to ZZe^+e^- \to e^+e^-b\bar{b}$. The signal characteristics change as a consequence: it is characterized by two forward (backward) energetic electrons (positrons), respectively, as shown in Figs. 11, 12, 13, and 19, and central,

less energetic, b jets, as depicted in Figs. 17 and 18.

The b jets of the background are mainly produced in the forward and backward directions (see Fig. 16). So at high energy, the signal characteristics confirm the dominance of the ZZ fusion Higgs production at high energies. This should be exploited to make maximal use of the high energy reach of ILC. This provides essential motivation to increase the energy after running at 250 GeV.

As a perspective, we can consider studying other processes with different final states [17, 18] and in other machines [19].

4. Appendix

CalcHEP is a package for the automatic calculation of elementary particle collisions and decays at the lowest order of perturbation theory (the tree approximation). It can be run in interactive or batch (non-interactive) modes. The interactive session of CalcHEP is graphical and menu-driven, guiding the user through the calculation by breaking it up into a series of steps. The batch session of CalcHEP is controlled by a set of scripts that perform common tasks non-interactively. Besides the standard model, CalcHEP has implemented many other models of particle interactions, such as the minimal supersymmetric extension of the standard model, the next-to-minimal supersymmetric extension of the standard model the Technicolor model, and the little Higgs model.

Example of a setup file (batch mode)

```
########################################
#  batch_file for CalcHEP              #
#  It has to be launched via           #
#          ./calchep_batch batch_file  #
# Lines beginning with # are ignored.  #
########################################
########################################
#              Model Info              #
#  Model is the exact model name.      #
#  Gauge specifies gauge. Choices are  #
#          Feynman or unitary.         #
########################################
Model: SM
Model changed: False
Gauge: Unitary
########################################
# Process Info                         #
# Process specifies the process.       #
########################################
Process: e,E->e,E,b,B
########################################
#              PDF Info                #
# ISR and Beamstrahlung are only available #
#          for electrons and positrons,  #
#          Default pdf: OFF            #
########################################
pdf1: OFF
pdf2: OFF
########################################
#  Momentum Info(center of mass energy) #
#              in GeV                  #
########################################
p1: 500
p2: 500
########################################
#        Physical_Parameters Info      #
########################################
Parameter: EE = 3.1343E-01
Parameter: Mb = 4.2500E+00
Parameter: MZ = 9.1188E+01
Parameter: MW = 8.0385E+01
Parameter: Mh = 1.2500E+02
Parameter: wZ = 2.49444E+00
Parameter: wW = 2.08895E+00
########################################
#              Cut Info                #
########################################
Cut parameter: M(b,B)
Cut invert: False
Cut min: 115
Cut max: 135
Cut parameter: T(e)
Cut invert: False
Cut min: 10
Cut max:
Cut parameter: T(E)
Cut invert: False
Cut min: 10
Cut max:
Cut parameter: M(e,E)
Cut invert:      False
Cut min:         20
Cut max:
########################################
#              Kinematics Info         #
########################################
Kinematics: 12 -> 34, 56
Kinematics: 34 -> 3, 4
Kinematics: 56 -> 5, 6
########################################
#           Regularization Info        #
```

```
########################################
Regularization momentum: 34
Regularization mass: MZ
Regularization width: wZ
Regularization power: 2
Regularization momentum: 56
Regularization mass: MZ
Regularization width: wZ
Regularization power: 2
Regularization momentum: 56
Regularization mass: Mh
Regularization width: wh
Regularization power: 2
########################################
#              Distribution Info       #
#   Only 1 dimensional distributions are #
#           currently supported.       #
########################################
Dist parameter: M(b,B)
Dist min:       0
Dist max:       500
Dist n bins:    300
Dist x-title:   M(b,B) (GeV)
Dist parameter: N(e)
Dist min:       -4
Dist max:       5
Dist n bins:    300
Dist x-title:   N(e) (GeV)
Dist parameter: N(E)
Dist min:       -4
Dist max:       5
Dist n bins:    300
Dist x-title:   N(E)
########################################
#              Vegas integration       #
#    nSess_1: number of the 1st sessions #
#  nCalls_1: number of calls per 1st sessions #
#   nSess_2: number of the 2nd sessions  #
# nCalls_2: number of calls per 2nd sessions #
########################################
nSess_1: 5
nCalls_1: 10000000
nSess_2: 5
nCalls_2: 10000000
```

References

[1] Aad, G. et al., Phys. Lett. B, 716 (2012) 1.

[2] Chatrchyan, S. et al., Phys. Lett. B, 716 (2012) 30.

[3] Azevedo, D., Ferreira, P., M¨uhlleitner, M.M., Santos, R., and Wittbrodt, J., Phys. Rev. D, 99 (2019) 055013.

[4] Asner, D.M. et al., arXiv:1310.0763 [hep-ph].

[5] van der Kolk, N., PoS DIS, 2016 (2016) 245.

[6] Kawada, S., PoS PANIC, 2021 (2022) 396.

[7] Tian, J. et al., PoS EPS-HEP, 2013 (2013) 316.

[8] Li, H. et al., arXiv:1202.1439 [hep-ex].

[9] Craig, N., Farina, M., McCullough, M., and Perelstein, M., J. High Energ. Phys. 146 (2015).

[10] Yan, J., Watanuki, S., Fujii, K., Ishikawa, A., Jeans, D., Strube, J., Tian, J., and Yamamoto, H., Phys. Rev. D, 94 (2016)113002.

[11] Ogawa, T., PoS ICHEP, 2018 (2019) 681.

[12] Drechsel, P., Moortgat-Pick, G., and Weiglein, G., Eur. Phys. J. C, 80 (10) (2020) 922.

[13] Jeans, D., PoS ICHEP, 2020 (2021) 057.

[14] Han, T., Liu, Z., Qian, Z., and Sayre, J., Phys. Rev. D, 91 (2015) 113007.

[15] Banerjee, S., Gupta, R.S., Ochoa-Valeriano, O. et al., J. High Energ. Phys., (2022) 176

[16] Belyaev, A., Christensen, N.D., and Pukhov, A., Comput. Phys. Commun., 184 (7) (2013) 1729.

[17] Antonov1, E. and Drutskoy1, A., Phys. Rev. D, 104 (2021) 093007.

[18] Yu, D., Ruan, M., Boudry, V. et al., Phys. J. C, 80 (2020) 7.

[19] de Blas, J., Cepeda, M., D'Hondt, J. et al., J. High Energ. Phys., (2020) 139.